Electronic Supplementary Material (ESI) for Environmental Science: Processes & Impacts.

Supplemental Information for:

Phase state of organic aerosols may limit temperature-driven thermodynamic repartitioning following outdoor-to-indoor transport

Bryan E. Cummings[1], Manabu Shiraiwa[2], Michael S. Waring[1,*]

[1]Drexel University, Philadelphia, Pennsylvania, USA
[2]University of California, Irvine, California, USA

[*]*Corresponding email:* msw59@drexel.edu

Contents

S1. IMAGES and indoor kinetic model details

IMAGES assumptions

- The volatility bins of the 2D-VBS are discretized in C^*_{298} at $\log_{10}$ intervals.
- The ideal mixing assumption is used when modeling under the VBS framework, so that $C^0 = C^*$ for the purposes of Equations 1 and 5 in the main text.
- IMAGES does not explicitly represent non-homogeneity of aerosol particles.
    1. Therefore, modeled $C_{OA(b)}$, D_b, and ρ_b in this work depend solely on the distribution of the particle-phase OM throughout the 2D-VBS and the amount of aerosol water in the mixture.

Kinetic partitioning details

- The vector version of $\boldsymbol{\varphi}$ is obtained via Equation 1 in the main text by using $\boldsymbol{C}^*$, $\boldsymbol{C}_g$, $\boldsymbol{C}_p$, and $\boldsymbol{k}_{gp}$ (each their respective vector forms). A vector version of $\boldsymbol{k}_{gp}$ is ultimately produced by utilizing $\boldsymbol{C}^*$ to compute $\boldsymbol{\alpha}$.
- The gas-phase parameters D_g and ω are not directly impacted by the bulk OA properties that IMAGES considers. Furthermore, indoor N_p and r_p values cannot be solved for directly without further resolving particle-phase OM into size bins in addition to volatility and O/C. Therefore, these four values were held constant at assumed values for any given model iteration

Indoor modeling approach

- In general, gas and particle source rates ($\boldsymbol{S}_g$, $\boldsymbol{S}_p$) may differ namely due to phase-dependent differences in outdoor concentrations, emission rates, and SOA formation. Further differences may also include envelope penetration or ventilation system filtration.
- Per Table 1 in the main text, the bulk OA viscosity (ν_b, Pa s) is informed from $T_{g(b)}$, the air temperature (T), and an estimate of the OA fragility using the modified Vogel-Tammann-Fulcher equation (Equation T1-10 in the main text).[1] Diffusivity is typically related to viscosity using the Stokes-Einstein equation (Equation T1-11 in the main text).[2] However, this may underpredict D_b for a relatively viscous OA matrix.[3] Since this is likely to be the case indoors,[4] the fractional Stokes-Einstein relationship was used instead.[5]
- Gas and particle loss rates (l_g, l_p) may differ due to deposition and filtration differences.
- For any organic compound parameter z that may be cast as functions of the 2D-VBS axes (z may be κ, ρ, or T_g in this study), its representative value for an OA particle (z_{org}) is simply the weighted average of all z_j, or its weighted average over all VBS bins, where each weight is the

particle mass fraction of either the compound or VBS bin j: $z_{org} = (C_p \cdot z)/C_{OA(org)}$, where " · " denotes the dot-product.

S2. Establishing outdoor OM

All outdoor OM was assumed to be at thermodynamic equilibrium immediately before it was transported indoors. Gas and particle OM concentration arrays ($\boldsymbol{C}_\mathrm{p}$, $\boldsymbol{C}_\mathrm{g}$) can be established based on this assumption, given: temperature (T), relative humidity (RH), and N number of OA factors, with each contributing an established ($C_{\mathrm{OA},i}$) concentration to the organic particle-phase concentration and possessing a fixed normalized OM distribution across VBS bins ($\boldsymbol{n}_i$). This procedure is as follows:

- The total absorbing mass of the bulk OA phase ($C_{\mathrm{OA(b)}}$) is:

$$C_{OA(b)} = C_{OA(org)} + C_{OA(w)} \qquad \text{S1}$$

  where $C_{\mathrm{OA(org)}}$ is the organic mass of the OA and $C_{\mathrm{OA(w)}}$ is the aerosol water mass taken up by the particle-phase organics. Based on the model inputs:

$$C_{OA(org)} = \sum_{i=1}^{N} C_{OA,i} \qquad \text{S2}$$

  Per the methods described in Section 2.2 and Table 1 in the main text, $C_{\mathrm{OA(w)}}$ is constrained according to κ-Köhler theory based on the average O/C of the total $\boldsymbol{C}_\mathrm{p}$ and the RH, as described in Section 2.2 in the main text.

- According to absorptive partitioning theory at thermodynamic equilibrium, the fraction of OM in each bin that is in the particle phase (i.e. the aerosol mass fraction; AMF; ξ) is:[6]

$$\xi = \left(1 + \frac{C^*}{C_{OA(b)}}\right)^{-1} \qquad \text{S3}$$

  where the $\boldsymbol{C}^*$ values have been shifted to account for temperature changes according to the Clausius-Clapeyron equation (Equation 7 in the main text).

- The normalized OM distribution for each factor was scaled to its total (gas + particle) OM concentration for each factor ($\boldsymbol{C}_i$) as:

$$C_i = \left(\frac{C_{OA,i}}{(\xi \bullet n_i)}\right) n_i \qquad \text{S4}$$

  where " • " denotes the dot product, and the term in the parenthetical serves as an effective scaling factor.

- The particle phase OM concentration for factor i is the element-wise product:

$$C_{p,i} = \xi C_i \tag{S5}$$

and the corresponding gas phase OM concentration is:

$$C_{g,i} = C_i - C_{p,i} \tag{S6}$$

The total gas- and particle-phase OM concentrations are simply:

$$C_p = \sum_{i=1}^{N} C_{p,i} \tag{S7}$$

$$C_g = \sum_{i=1}^{N} C_{g,i} \tag{S8}$$

- Because $\boldsymbol{C}_{\mathrm{p}}$ and $C_{\mathrm{OA(w)}}$ are co-dependent, $\boldsymbol{C}_{\mathrm{p}}$ (and all $\boldsymbol{C}_{\mathrm{p},i}$) must be solved for iteratively after an initial guess for the value of $C_{\mathrm{OA(w)}}$. Assuming no aerosol water initially will still yield rapid convergence.

For the parametric analysis, only one outdoor OA factor was simulated at a time (i.e. $N = 1$), being either TOA, HOA, or OOA. For the climate zone analysis, all outdoor OA was resolved into three factors ($N = 3$), being HOA, SVOOA, and LVOOA. The normalized $\boldsymbol{n}_i$ distributions for all factors are listed in Table S1. For all simulations, the final $\boldsymbol{C}_{\mathrm{p}}$ and $\boldsymbol{C}_{\mathrm{g}}$ terms outputted by Equations S7 and S8 are inserted into Equations 10 and 11 in the main text as C_p^{out} and C_g^{out} in the main text, respectively.

Table S1. For five OA factors considered in this work, O/C values and volatility distributions of OM (from the literature[7,8]) corresponding to its outdoor condition before being transformed by mechanical losses and repartitioning.

Factor	O/C	$\log_{10} C^*_{298}$ (μg/m³)										
		–7	–6	–5	–4	–3	–2	–1	0	1	2	3
TOA	0.51	-	0.035	0.036	0.036	0.037	0.038	0.043	0.056	0.091	0.186	0.443
HOA	0.13	-	0.015	0.016	0.018	0.021	0.028	0.041	0.067	0.121	0.228	0.445
OOA	0.64	-	0.066	0.066	0.067	0.068	0.069	0.074	0.083	0.104	0.150	0.253
SVOOA	0.51	-	-	0.043	0.050	0.059	0.072	0.089	0.113	0.144	0.187	0.244
LVOOA	0.81	0.315	0.217	0.150	0.104	0.071	0.050	0.034	0.024	0.016	0.011	0.008

S3. Indoor parameters used in the Monte Carlo simulations

Primary variables

Indoor and building-related model inputs were sampled from probability distributions (Table S2). Natural ventilation was not resolved from infiltration for residences, so a combined $\lambda_i + \lambda_n$ distribution was defined, and an effective total particle penetration factor $p = 0.95$ was set. Particle filtration by forced-air recirculation HVAC systems was explicitly modeled, so k_{dep} only accounts for deposition onto indoor surfaces for simulations study 2. Since size-dependent particle dynamics cause deposition rates onto filters and surfaces to covary, k_{dep} was computed as a function of the sampled η.[9] The fractional runtimes (f_{RT}) of residential HVAC systems were varied according to the outdoor temperature.[10] N_p and r_p were each maintained at 5000 cm^{-3} and 0.1 µm, respectively, for all model instances.

These parameters and distributions were constant for all climate zones and seasons that were simulated. In reality, infiltration air exchange will vary with outdoor temperature and the housing stock will vary with climate. However, temperature-based differences in infiltration rates are assumed to have a small effect on the repartitioning regime compared to the effect of statistical noise among other housing stock characteristics, the temperature gradient, and the effective water activity, so it was not modeled explicitly in this study.

Table S2. Distribution definitions for randomly sampled building model inputs.

Parameter	Units	Distribution			Max	Ref.
		Type	A	B		
T_{in}	K	N	296.9	3	-	[11,12]
$\lambda_i + \lambda_n$	h^{-1}	LN	0.75	2.1	-	[11,12]
λ_r	h^{-1}	LN	6.4	1.63	-	[13]
η	-	LN	0.2	2.4	0.95	[14]

N = Normal; A = mean; B = standard deviation
LN = Lognormal; A = geometric mean; B = geometric standard deviation

Secondary variables

(*The following descriptions were adopted directly from the SI of Cummings et al.*[4])

Surface deposition rate

Rackes and Waring[9] produced a second order polynomial expression for PM surface deposition (k_{dep}, h^{-1}) as a function of the HVAC filtration rate (η):

$$k_{dep} = 0.171\eta^2 - 0.1378\eta + 0.0918 \quad \text{S9}$$

This was shown to produce a good fit with an $R^2 = 0.983$. This empirical relationship was used to constrain k_{dep} in the model after η was sampled from its input distribution.

HVAC runtime

The fractional runtime of the residential HVAC recirculation system (f_{RT}) was derived from the work of Touchie and Seigel[10]. They measured f_{RT} for ~7000 homes in North America and plotted them against the outdoor temperature (T_{out}, °C). They also provided linear equations of best fit for both cooling and heating conditions:

$$f_{RT,heat} = -0.0068T_{out} + 0.207 \quad \text{S10}$$

$$f_{RT,cool} = 0.0112T_{out} + 0.0277 \quad \text{S11}$$

In this work, heating was enforced anytime $T_{out} < 15$ °C, and cooling was enforced anytime $T_{out} > 21$ °C. Although Touchie and Seigel[10] often observed recirculation systems operating at low frequencies within this deadband zone, for simplicity in our work, no recirculation was assumed (i.e. $f_{RT} = 0$) if T_{out} was between the enforced deadband.

Indoor RH

Nguyen et al.[15] found this relationship between outdoor and indoor absolute humidity (AH, g/m^3):

$$AH_{in} = 0.69AH_{out} + 3.2 \quad \text{S12}$$

to best describe their observations of homes in Boston ($R^2 = 0.83$). By visual inspection, this parameterization also fit the trends observed by Nguyen and Dockery[16] for multiple cities reasonably well. For homes in hot and humid cities that employed air conditioning, Figure 3 in Nguyen and Dockery[16] showed that increases in AH_{in} with increasing AH_{out} were diminished at higher AH values, deviating from the relation of Equation S12. This occurrence was attributed to loss of water vapor via condensation over cooling coils.

Our procedure for constraining the indoor RH was informed by this set of observation, and is as follows:

1. RH_{out} was appropriately converted to AH considering T_{out}.
2. This AH_{out} was fed to Equation S12 to obtain a first-estimate of AH_{in}.
3. Statistical variation was simulated by sampling a residual to be applied to the AH_{in} predicted by Step 2 from a normal distribution.

4. If cooling is being provided, the additional loss rate of water (g m^{-3} h^{-1}) from the airstream would be proportional to the recirculation AER (λ_r, h^{-1}), f_{RT}, and the AH, and so the AH_{in} predicted by Step 3 would be reduced proportionally to this loss rate.
5. The final AH_{in} was appropriately converted to RH considering T_{in}.
6. Since this approach is statistical, not physical, some RH_{in} may be greater than 100%. Any RH_{in} values above 95% were truncated to 95%.

This procedure, as it relates to AH, is encapsulated by the following equation:

$$AH_{in} = 0.69AH_{out} + 3.2 + N(0, \sigma) + \alpha f_{RT,cool}\lambda_r AH_{out} \tag{S13}$$

Where:

- The first two terms account for the Nguyen et al.[15] relationship from Equation S12, the third terms accounts for statistical variability, and the fourth term accounts for coil loss proportional to a constant, α, and the flow rate of water over the coil (using AH_{out} rather than AH_{in} in this fourth term simplifies the required math and provides a good enough water loss proxy for our purposes).
- $N(0, \sigma)$ represents a random sample from a normal distribution defined with a mean of zero and standard deviation of σ. To avoid negative numbers and extreme outliers, only samples within the 95% confidence interval of this distribution were allowed.
- When $T_{out} > 21$ °C, $f_{RT,cool}$ is governed by Equation S11; and $f_{RT,cool} = 0$ any time $T_{out} \leq 21$ °C.
- Per engineering judgement, we deemed $\sigma = 0.5$, and $\alpha = -0.06$.

The progression of this procedure is shown in Figure S1 as it relates to all 9938 of our model instances. All AH_{out} values used in our simulations are scattered against:

i. (Figure S1a) the AH_{in} predicted by the simple linear Equation S12.
ii. (Figure S1b) the AH_{in} values adjusted by Step 3.
iii. (Figure S1c) all final AH_{in} values used to obtain RH_{in} including water loss adjustments by Step 4 as appropriate.

The AH_{in} values appropriately converted to RH_{in} according to T_{out} are shown in Figure S2 as a histogram. Of the 9938 instances, this procedure only yielded 18 that initially produced RH_{in} > 100%. However, for additional stability of our results, we truncated the maximum allowed RH_{in} for IMAGES to consider to be 95%. Ultimately, this methodology produced 35 cases that required such truncation.

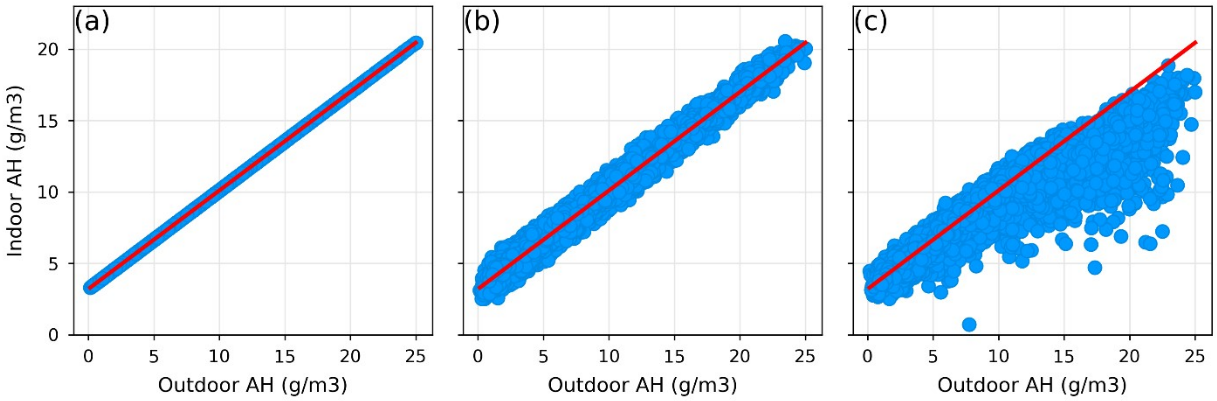

Figure S1. AH_{in}-AH_{out} scatter plots over all 9938 model instances showing the AH_{in} predicted by: **(a)** the Equation S12 from Nguyen et al.[15]; **(b)** the Equation S12 prediction including random variability; and **(c)** the final prediction including random variability and water loss to an operational cooling coil. The red line overlaid on each plot is the line produced by Equation S12, shown for reference. The points in pane **(c)** match in decent accordance with the observations made by Nguyen and Dockery[16] that were presented in their Figure 3.

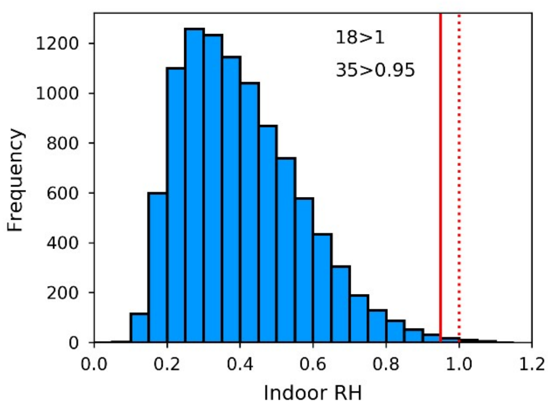

Figure S2. A histogram of the RH_{in} values converted from the AH_{in} values shown in Figure S1c. RH = 100% is marked with the dotted red line, and RH = 95% is marked with the solid red line. RH_{in} can never actually reach values greater than 100%, and this method only produced 18 of 9938 instances where this occurred. For further stability, we truncated the maximum possibile RH_{in} that IMAGES considered in these simulations to be 95%, which the methodology produced in 35 of the 9938 instances.

S4. Mechanical-only model framework

This model framework treats all OA as static particles that do not exhibit any semivolatile behavior. No discretization of OM is therefore needed and gaseous OM can be neglected, since the VBS framework is not utilized. Instead, mechanical-only model indoor OA concentrations of outdoor origin (C^{mech}_{OA}) are described with:

$$C^{mech}_{OA} = (\lambda_n + (1 - \eta)\lambda_v + p\lambda_i)C^{out}_{OA} - (\lambda_{tot} + f_{RT}\lambda_r\eta + k_{dep})C^{mech}_{OA} \qquad \text{S14}$$

where C^{mech}_{OA} (μg/m^3) is the outdoor particle-phase OA concentration; λ_v, λ_n, and λ_i (h^{-1}) denote the mechanical ventilation, natural ventilation, and infiltration air exchange rates (AER), respectively, and the total outdoor AER (λ_{tot}) is the sum $\lambda_v + \lambda_n + \lambda_i$; η is the particle filter efficiency; and p is the penetration factor of infiltrating particles; k_{dep}, (h^{-1}) is the indoor surface deposition loss rate coefficient, λ_r (h^{-1}) is the recirculation AER; and f_{RT} is the fractional runtime of the recirculation system.

S5. Equilibrium model framework

The equilibrium thermodynamic model is built upon the same VBS foundational framework as the kinetic model described in Section 2.2 of the main text. However, instead of modeling gas- and particle-phase OM as separate systems that may exchange material according to a designated rate of partitioning, all gas + particle OM at equilibrium are lumped into a single array of VBS bins ($\boldsymbol{C}^{eq}$).

At equilibrium, the absorptive theory of thermodynamic partitioning prescribes the aerosol mass fraction (AMF), which defines the fraction of OM in each bin that resides in the particle-phase, as:[6]

$$\xi = \left(1 + \frac{C^*}{C_{OA(b)}^{eq}}\right)^{-1} \qquad \text{S15}$$

where $\boldsymbol{\xi}$ is the equilibrium AMF in all VBS bins; $C_{OA(b)}^{eq}$ is the total absorbing mass of the bulk OA; and $\boldsymbol{C}^*$ is the effective saturation concentration, shifted to account for temperature changes according to the Clausius-Clapeyron equation (Equation 7 in the main text). $C_{OA(b)}^{eq}$ is defined according to the analogous Equation T1-1 in the main text, and the element-wise product:

$$C_p^{eq} = \xi C^{eq} \qquad \text{S16}$$

yields the particle-phase OM concentration in the VBS at equilibrium (C_p^{eq}).

The total equilibrium OM concentration indoors is governed by: $\frac{dC^{eq}}{dt} = (\lambda_n + (1 - \eta)\lambda_v + p\lambda_i)C_p^{out} + \lambda_{tot}C_g^{out} - ((\lambda_{tot} + f_{RT}\lambda_r r$

where C_p^{out} and C_g^{out} are established according to the methods described in Section S1 in this SI.

S6. Non-continuum effects

When assuming ideal mass accommodation (and assuming $D_g = 0.1$ cm^2/s and $\omega = 2\times10^4$ cm/s for computing the Knudsen number), $r_p > 1$ µm produces $\beta \approx 1$ while smaller r_p values produce proportionally small β values, illustrating the effects of non-continuum fluid flow. This may impede gas-to-particle partitioning for small particles (e.g. Figure 1e in the main text).

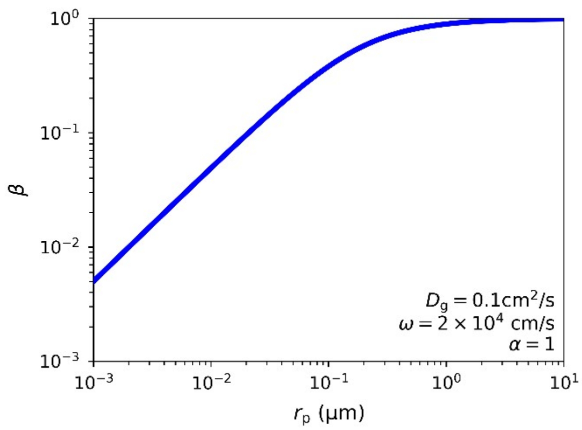

Figure S3. β (per Equations 3 and 4 in the main text) as a function of r_p assuming $\alpha = 1$, $D_g = 0.1$ cm^2/s, and $\omega = 2\times10^4$ cm/s.

S7. HOA and OOA bulk diffusivity

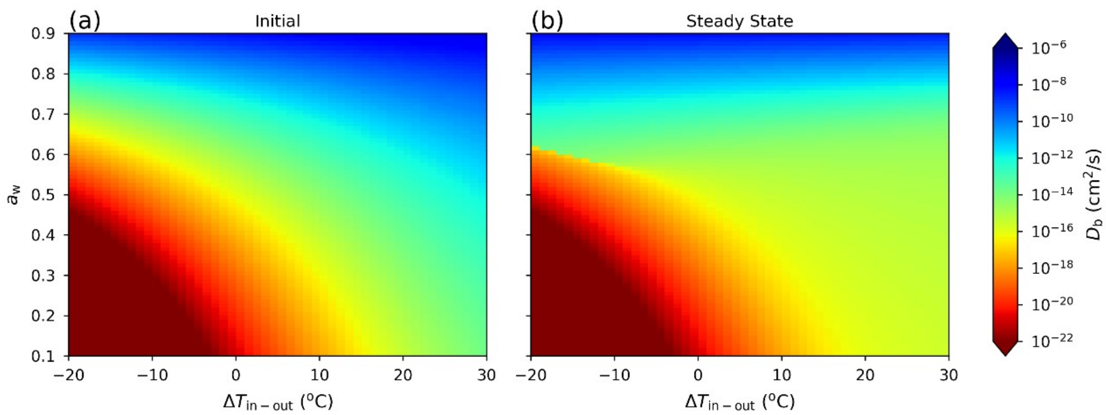

Figure S4. For HOA simulated under the parametric analysis, Indoor D_b as a function of ΔT and RH **(a)** immediately upon outdoor-to-outdoor transport (after the ambient OA has taken on its indoor phase state but before and OM has partitioned) and **(b)** after steady state conditions have been established.

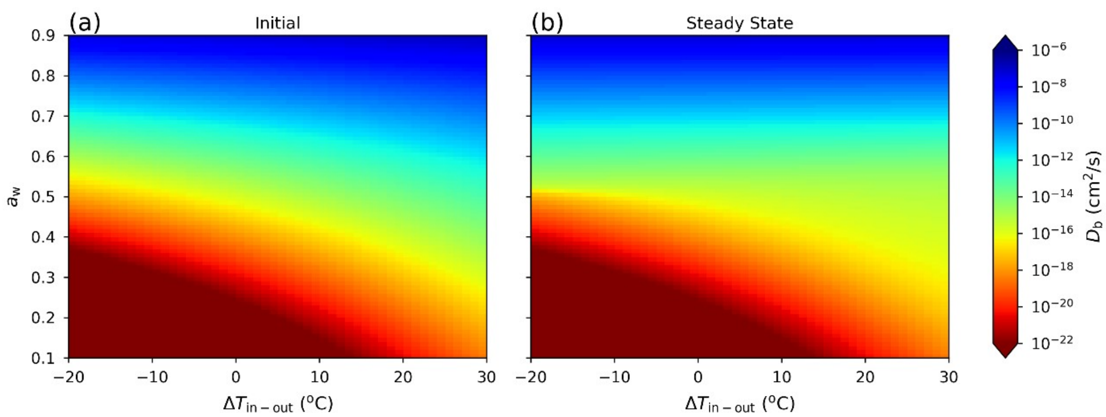

Figure S5. For OOA simulated under the parametric analysis, Indoor D_b as a function of ΔT and RH **(a)** immediately upon outdoor-to-outdoor transport (after the ambient OA has taken on its indoor phase state but before and OM has partitioned) and **(b)** after steady state conditions have been established.

S8. Outdoor temperature impact on outdoor OM volatility distribution

When holding C_{OA} and the OA factor (i.e. volatility distribution) constant, T can significantly affect the distribution of $\boldsymbol{C}_p$ according to the VBS model at equilibrium (Figure S6). A lower T overrepresents higher-volatility molecules in the particle-phase, so the average C^*_{298} of the bulk particle will be high and, at room temperature, the OA matrix will be less viscous. This explains the phenomenon observed in the main text, where the a_w threshold for nonvolatile behavior decreases as T_{out} decreases.

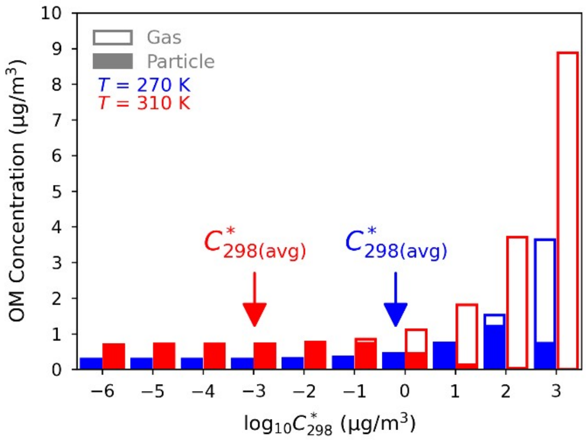

Figure S6. 5 μg/m³ of particle-phase TOA at equilibrium at T = 270 K and T = 310 K.

S9. Additional insight provided by Monte Carlo summary statistics

The following points provide further details from analysis of Table 4 in the main text.

Manifestation of cases under condensing conditions

- The distribution of cases among condensation categories was bimodal. Both phase transition assumption simulation sets experienced only tens of cases of partial condensation. This is consistent with the observations of Section 3.1.1 and the analysis provided in Sections 3.1.2 in the main text.
- T_{out} was used to compute D_b ($T = T_{out}$ for Equations T1-10 and T1-11) for the slow-phase-transition group when $\Delta T_{in\text{-}out} < 0$. This was responsible for shifting the distribution of cases modestly toward equilibrium condensation instead of prohibited condensation, compared to the rapid-phase-transition simulations. However, this impact of varying T was smaller than the impact of varying a_w under this model domain with respect to the D_b calculation.

Under what conditions does the slow-phase-transition assumption produce prohibited evaporation? Where in the U.S. do these conditions arise?

- Nearly all model instances in the simulated humid (A), uncategorized, or marine (C) climate zone groupings possessed average RH_{out} values in the 60–70% range in the winter (Table 3 in the main text). So, most slow-phase-transition assumption cases that produced prohibited evaporation occurred within the warm and arid (B) climate zone grouping, where RH_{out} was frequently below 50% in the winter. This occurrence also manifests in the $\Delta T_{in\text{-}out}$ characteristics for slow-phase-transition nonvolatile behavior. Its average value is much smaller compared to the partial and equilibrium $\Delta T_{in\text{-}out}$ values for evaporative conditions, meaning that the warmer outdoors representative of desert climates mostly corresponds to the nonvolatile behavior, while simulated evaporation occurred under the cooler, upper-latitude coastal conditions.

Analysis of partitioning factors

- By definition, $F \approx 1$ for the two categorizations where repartitioning was kinetically prohibited indoors and also when $\Delta T_{in\text{-}out} \approx 0$, regardless of the phase transition assumption.
- F behavior belonging to each condensation categorization was similar between the rapid-phase-transition and slow-phase-transition simulation sets, while the phase transition assumption caused more divergent outcomes in cases of evaporation.
- Either phase transition assumptions of both partial and equilibrium condensation saw predominantly modest increases in OA concentration relative to nonvolatile particles; about a 10% ($F \approx 1.1$) average increase was realized.

- By assuming a slow phase transition, OA undergoing partial evaporation experienced, on average, a 17% loss in mass ($F = 0.83$), and equilibrium evaporation was associated with an average loss of mass equal to 21% ($F = 0.79$) with a somewhat larger standard deviation. In some cases of equilibrium evaporation, the OA mass was reduced by roughly a factor of two.
- Considerably different F behavior among the evaporative repartitioning categorizations was produced for a rapid phase transition; both partial and equilibrium evaporation led to the similar average F values of 0.92 and 0.93, respectively.

S10. Isolating the effect of housing stock and aerosol features on repartitioning

Figure S7 plots the coefficient of variance of the F values for similar temperature gradient and water activity conditions corresponding to Figures 3a and 3b in the main text. In any given season for a particular location, most of the variability in the simulated partitioning regime and F are due to day-to-day differences in meteorological conditions. However, for similar meteorological conditions (i.e., similar $\Delta T_{\text{in-out}}$ and a_w), variability is due to differences in the housing stock (e.g. airflow, deposition) or aerosol characteristics (e.g. semivolatility of chemical constituents), which is illustrated here. Variability does not emerge for the prohibited repartitioning regime since the aerosol diffusivity forces $F \approx 1$ regardless of the environmental conditions. Under conditions that are conducive to repartitioning, a 15-20% variability of F values was common for a given $\Delta T_{\text{in-out}}$ and a_w combination.

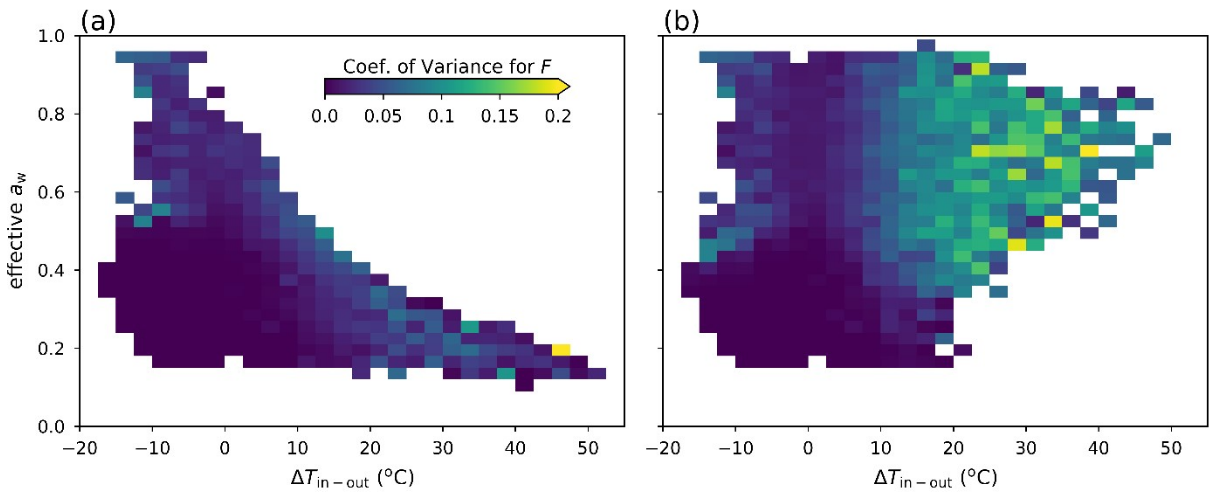

Figure S7. For the rapid- **(a)** and slow- **(b)** phase-transition assumptions, the coefficient of variance of the modeled F values are plotted as a function of the temperature gradient and the effective a_w.

S11. Tabulation of main text Figure 4.

Summer, rapid phase transition

Table S3. Frequency (total number) of rapid-phase-transition simulations being classified according to the listed repartitioning designation occurring for each climate zone in the summertime (June + July + August). This data corresponds to Figure 4a in the main text.

		Percent of City+Season Simulations (Total Number of Simulations)						
Climate Zone	City	Equilibrium Condensation	Partial Condensation	Prohibited Condensation	No Appreciable Temperature Gradient	Prohibited Evaporation	Partial Evaporation	Equilibrium Evaporation
Humid/Uncategorized								
1A	Miami	62.58% (97)	2.58% (4)	9.68% (15)	21.94% (34)	1.29% (2)	0.65% (1)	1.29% (2)
2A	Houston	68.9% (144)	2.39% (5)	8.61% (18)	15.79% (33)	1.44% (3)	0.0% (0)	2.87% (6)
3A	Atlanta	42.01% (71)	4.14% (7)	15.98% (27)	23.08% (39)	9.47% (16)	1.18% (2)	4.14% (7)
4A	Baltimore	29.19% (54)	0.0% (0)	9.19% (17)	28.11% (52)	27.57% (51)	2.16% (4)	3.78% (7)
5A	Chicago	16.57% (30)	1.1% (2)	3.87% (7)	29.28% (53)	38.67% (70)	6.08% (11)	4.42% (8)
6A	Milwaukee	13.64% (27)	0.0% (0)	4.55% (9)	24.24% (48)	39.9% (79)	5.56% (11)	12.12% (24)
7	Fargo	12.72% (22)	0.0% (0)	4.05% (7)	26.01% (45)	43.93% (76)	6.94% (12)	6.36% (11)
8	Fairbanks	3.95% (3)	0.0% (0)	1.32% (1)	2.63% (2)	61.84% (47)	23.68% (18)	6.58% (5)
Arid								
2B	Phoenix	9.62% (20)	5.29% (11)	83.17% (173)	1.44% (3)	0.48% (1)	0.0% (0)	0.0% (0)
3B	Las Vegas	2.6% (4)	0.65% (1)	94.81% (146)	1.95% (3)	0.0% (0)	0.0% (0)	0.0% (0)
4B	Albuquerque	3.41% (6)	0.57% (1)	53.98% (95)	23.86% (42)	18.18% (32)	0.0% (0)	0.0% (0)
5B	Denver	2.15% (2)	2.15% (2)	22.58% (21)	16.13% (15)	51.61% (48)	5.38% (5)	0.0% (0)
6B	Helena	0.0% (0)	0.0% (0)	8.0% (10)	23.2% (29)	67.2% (84)	1.6% (2)	0.0% (0)
Marine								
3Bc	Los Angeles	2.44% (3)	0.0% (0)	0.81% (1)	22.76% (28)	34.96% (43)	11.38% (14)	27.64% (34)
3C	San Jose	7.02% (12)	0.58% (1)	2.92% (5)	21.64% (37)	57.31% (98)	2.34% (4)	8.19% (14)
4C	Seattle	0.58% (1)	0.58% (1)	5.23% (9)	17.44% (30)	60.47% (104)	9.3% (16)	6.4% (11)

Spring/Fall, rapid phase transition

Table S4. Frequency (total number) of rapid-phase-transition simulations being classified according to the listed repartitioning designation occurring for each climate zone in the summertime (March + April + May + September + October + November). This data corresponds to Figure 4b in the main text.

		Percent of City+Season Simulations (Total Number of Simulations)						
Climate Zone	City	Equilibrium Condensation	Partial Condensat ion	Prohibited Condensation	No Appreciable Temperature Gradient	Prohibited Evaporation	Partial Evaporation	Equilibrium Evaporation
Humid/Uncategorized								
1A	Miami	40.24% (136)	0.0% (0)	5.62% (19)	34.02% (115)	18.05% (61)	0.3% (1)	1.78% (6)
2A	Houston	21.7% (87)	0.0% (0)	2.49% (10)	23.44% (94)	36.91% (148)	5.24% (21)	10.22% (41)
3A	Atlanta	10.27% (34)	0.6% (2)	1.81% (6)	12.08% (40)	59.52% (197)	7.85% (26)	7.85% (26)
4A	Baltimore	3.52% (12)	0.0% (0)	1.47% (5)	7.92% (27)	66.28% (226)	15.54% (53)	5.28% (18)
5A	Chicago	1.14% (4)	0.0% (0)	0.86% (3)	4.29% (15)	79.43% (278)	10.0% (35)	4.29% (15)
6A	Milwaukee	2.05% (8)	0.0% (0)	0.0% (0)	4.36% (17)	82.05% (320)	6.92% (27)	4.62% (18)
7	Fargo	1.11% (4)	0.0% (0)	0.0% (0)	4.99% (18)	89.47% (323)	3.6% (13)	0.83% (3)
8	Fairbanks	0.0% (0)	0.0% (0)	0.0% (0)	0.67% (1)	81.21% (121)	18.12% (27)	0.0% (0)
Arid								
2B	Phoenix	1.79% (7)	1.02% (4)	45.01% (176)	15.6% (61)	34.78% (136)	1.79% (7)	0.0% (0)
3B	Las Vegas	0.74% (2)	0.0% (0)	28.31% (77)	12.13% (33)	57.35% (156)	1.1% (3)	0.37% (1)
4B	Albuquerque	0.29% (1)	0.0% (0)	3.5% (12)	5.83% (20)	86.59% (297)	3.5% (12)	0.29% (1)
5B	Denver	0.0% (0)	0.0% (0)	0.56% (1)	2.79% (5)	88.83% (159)	6.7% (12)	1.12% (2)
6B	Helena	0.0% (0)	0.0% (0)	0.0% (0)	0.39% (1)	98.82% (251)	0.39% (1)	0.39% (1)
Marine								
3Bc	Los Angeles	2.36% (5)	0.47% (1)	3.77% (8)	7.08% (15)	54.25% (115)	20.75% (44)	11.32% (24)
3C	San Jose	0.62% (2)	0.0% (0)	2.18% (7)	9.66% (31)	66.67% (214)	14.64% (47)	6.23% (20)
4C	Seattle	0.0% (0)	0.0% (0)	0.3% (1)	1.52% (5)	64.33% (211)	29.57% (97)	4.27% (14)

Winter, rapid phase transition

Table S5. Frequency (total number) of rapid-phase-transition simulations being classified according to the listed repartitioning designation occurring for each climate zone in the summertime (December + January + February). This data corresponds to Figure 4c in the main text.

Climate Zone	City	Percent of City+Season Simulations (Total Number of Simulations)						
		Equilibrium Condensation	Partial Condensation	Prohibited Condensation	No Appreciable Temperature Gradient	Prohibited Evaporation	Partial Evaporation	Equilibrium Evaporation
Humid/Uncategorized								
1A	Miami	17.57% (26)	0.68% (1)	2.03% (3)	22.97% (34)	44.59% (66)	6.76% (10)	5.41% (8)
2A	Houston	0.51% (1)	0.0% (0)	0.0% (0)	5.58% (11)	71.07% (140)	11.17% (22)	11.68% (23)
3A	Atlanta	0.66% (1)	0.0% (0)	0.0% (0)	0.0% (0)	72.85% (110)	23.18% (35)	3.31% (5)
4A	Baltimore	0.0% (0)	0.0% (0)	0.0% (0)	0.0% (0)	83.23% (139)	16.17% (27)	0.6% (1)
5A	Chicago	0.0% (0)	0.0% (0)	0.0% (0)	0.0% (0)	84.81% (134)	15.19% (24)	0.0% (0)
6A	Milwaukee	0.0% (0)	0.0% (0)	0.0% (0)	0.0% (0)	97.97% (193)	2.03% (4)	0.0% (0)
7	Fargo	0.0% (0)	0.0% (0)	0.0% (0)	0.0% (0)	97.85% (182)	2.15% (4)	0.0% (0)
8	Fairbanks	0.0% (0)	0.0% (0)	0.0% (0)	0.0% (0)	66.2% (47)	33.8% (24)	0.0% (0)
Arid								
2B	Phoenix	0.52% (1)	0.0% (0)	1.55% (3)	4.12% (8)	72.68% (141)	20.62% (40)	0.52% (1)
3B	Las Vegas	0.0% (0)	0.0% (0)	0.0% (0)	0.69% (1)	66.67% (96)	32.64% (47)	0.0% (0)
4B	Albuquerque	0.0% (0)	0.0% (0)	0.0% (0)	0.0% (0)	60.47% (104)	39.53% (68)	0.0% (0)
5B	Denver	0.0% (0)	0.0% (0)	0.0% (0)	0.0% (0)	55.81% (48)	44.19% (38)	0.0% (0)
6B	Helena	0.0% (0)	0.0% (0)	0.0% (0)	0.0% (0)	93.97% (109)	6.03% (7)	0.0% (0)
Marine								
3Bc	Los Angeles	0.94% (1)	0.0% (0)	0.0% (0)	0.94% (1)	49.06% (52)	47.17% (50)	1.89% (2)
3C	San Jose	0.0% (0)	0.0% (0)	0.0% (0)	0.62% (1)	32.3% (52)	63.98% (103)	3.11% (5)
4C	Seattle	0.0% (0)	0.0% (0)	0.0% (0)	0.0% (0)	45.16% (70)	54.19% (84)	0.65% (1)

Summer, slow phase transition

Table S6. Frequency (total number) of slow-phase-transition simulations being classified according to the listed repartitioning designation occurring for each climate zone in the summertime (June + July + August). This data corresponds to Figure 4d in the main text.

		Percent of City+Season Simulations (Total Number of Simulations)						
Climate Zone	City	Equilibrium Condensation	Partial Condensation	Prohibited Condensation	No Appreciable Temperature Gradient	Prohibited Evaporation	Partial Evaporation	Equilibrium Evaporation
Humid/Uncategorized								
1A	Miami	83.23% (129)	0.0% (0)	0.0% (0)	14.84% (23)	0.0% (0)	0.0% (0)	1.94% (3)
2A	Houston	86.6% (181)	0.48% (1)	0.96% (2)	10.53% (22)	0.0% (0)	0.0% (0)	1.44% (3)
3A	Atlanta	61.54% (104)	1.78% (3)	2.96% (5)	23.67% (40)	0.0% (0)	0.0% (0)	10.06% (17)
4A	Baltimore	42.16% (78)	1.08% (2)	1.62% (3)	25.41% (47)	2.7% (5)	0.54% (1)	26.49% (49)
5A	Chicago	24.86% (45)	0.55% (1)	1.66% (3)	27.07% (49)	2.76% (5)	8.84% (16)	34.25% (62)
6A	Milwaukee	19.19% (38)	0.51% (1)	1.52% (3)	26.26% (52)	1.01% (2)	3.54% (7)	47.98% (95)
7	Fargo	16.76% (29)	0.58% (1)	0.58% (1)	30.06% (52)	1.73% (3)	6.36% (11)	43.93% (76)
8	Fairbanks	3.95% (3)	0.0% (0)	1.32% (1)	3.95% (3)	10.53% (8)	11.84% (9)	68.42% (52)
Arid								
2B	Phoenix	24.04% (50)	7.69% (16)	66.35% (138)	1.92% (4)	0.0% (0)	0.0% (0)	0.0% (0)
3B	Las Vegas	5.19% (8)	3.9% (6)	88.96% (137)	1.95% (3)	0.0% (0)	0.0% (0)	0.0% (0)
4B	Albuquerque	8.52% (15)	1.7% (3)	48.86% (86)	22.73% (40)	13.07% (23)	1.7% (3)	3.41% (6)
5B	Denver	5.38% (5)	3.23% (3)	18.28% (17)	21.51% (20)	25.81% (24)	10.75% (10)	15.05% (14)
6B	Helena	0.0% (0)	0.8% (1)	7.2% (9)	22.4% (28)	54.4% (68)	3.2% (4)	12.0% (15)
Marine								
3Bc	Los Angeles	5.69% (7)	0.0% (0)	0.0% (0)	21.95% (27)	0.0% (0)	0.0% (0)	72.36% (89)
3C	San Jose	8.77% (15)	0.0% (0)	1.75% (3)	22.81% (39)	1.75% (3)	1.75% (3)	63.16% (108)
4C	Seattle	1.16% (2)	0.58% (1)	4.07% (7)	20.35% (35)	5.23% (9)	4.65% (8)	63.95% (110)

Spring/Fall, slow phase transition

Table S7. Frequency (total number) of slow-phase-transition simulations being classified according to the listed repartitioning designation occurring for each climate zone in the summertime (March + April + May + September + October + November). This data corresponds to Figure 4e in the main text.

		Percent of City+Season Simulations (Total Number of Simulations)						
Climate Zone	City	Equilibrium Condensation	Partial Condensation	Prohibited Condensation	No Appreciable Temperature Gradient	Prohibited Evaporation	Partial Evaporation	Equilibrium Evaporation
Humid/Uncategorized								
1A	Miami	53.85% (182)	0.0% (0)	0.59% (2)	28.7% (97)	1.78% (6)	0.59% (2)	14.5% (49)
2A	Houston	27.43% (110)	0.5% (2)	0.5% (2)	23.94% (96)	6.23% (25)	4.24% (17)	37.16% (149)
3A	Atlanta	13.29% (44)	0.0% (0)	0.0% (0)	14.2% (47)	12.39% (41)	16.31% (54)	43.81% (145)
4A	Baltimore	4.69% (16)	0.0% (0)	0.59% (2)	9.38% (32)	12.32% (42)	20.23% (69)	52.79% (180)
5A	Chicago	1.71% (6)	0.0% (0)	0.29% (1)	5.71% (20)	7.43% (26)	21.43% (75)	63.43% (222)
6A	Milwaukee	2.05% (8)	0.0% (0)	0.0% (0)	5.13% (20)	6.15% (24)	18.72% (73)	67.95% (265)
7	Fargo	1.39% (5)	0.0% (0)	0.0% (0)	4.71% (17)	12.74% (46)	16.34% (59)	64.82% (234)
8	Fairbanks	0.0% (0)	0.0% (0)	0.0% (0)	0.67% (1)	14.09% (21)	27.52% (41)	57.72% (86)
Arid								
2B	Phoenix	3.84% (15)	2.05% (8)	41.94% (164)	15.6% (61)	29.67% (116)	5.12% (20)	1.79% (7)
3B	Las Vegas	2.21% (6)	0.37% (1)	26.47% (72)	12.13% (33)	54.04% (147)	2.21% (6)	2.57% (7)
4B	Albuquerque	0.58% (2)	0.0% (0)	3.5% (12)	5.83% (20)	64.72% (222)	14.87% (51)	10.5% (36)
5B	Denver	0.0% (0)	0.0% (0)	0.56% (1)	2.79% (5)	34.08% (61)	35.2% (63)	27.37% (49)
6B	Helena	0.0% (0)	0.0% (0)	0.0% (0)	0.79% (2)	39.37% (100)	23.23% (59)	36.61% (93)
Marine								
3Bc	Los Angeles	4.25% (9)	0.0% (0)	2.83% (6)	7.08% (15)	4.72% (10)	8.02% (17)	73.11% (155)
3C	San Jose	0.93% (3)	0.31% (1)	1.87% (6)	10.9% (35)	7.48% (24)	11.84% (38)	66.67% (214)
4C	Seattle	0.0% (0)	0.0% (0)	0.3% (1)	1.52% (5)	3.66% (12)	7.01% (23)	87.5% (287)

Winter, slow phase transition

Table S8. Frequency (total number) of slow-phase-transition simulations being classified according to the listed repartitioning designation occurring for each climate zone in the summertime (December + January + February). This data corresponds to Figure 4f in the main text.

Climate Zone	City	Percent of City+Season Simulations (Total Number of Simulations)						
		Equilibrium Condensation	Partial Condensa tion	Prohibite d Condensa tion	No Appreciable Temperature Gradient	Prohibited Evaporation	Partial Evaporation	Equilibrium Evaporation
Humid/Uncategorized								
1A	Miami	20.95% (31)	0.0% (0)	0.0% (0)	28.38% (42)	1.35% (2)	12.84% (19)	36.49% (54)
2A	Houston	0.51% (1)	0.0% (0)	0.0% (0)	7.11% (14)	3.55% (7)	14.72% (29)	74.11% (146)
3A	Atlanta	0.66% (1)	0.0% (0)	0.0% (0)	0.0% (0)	3.31% (5)	43.05% (65)	52.98% (80)
4A	Baltimore	0.0% (0)	0.0% (0)	0.0% (0)	0.0% (0)	1.8% (3)	37.72% (63)	60.48% (101)
5A	Chicago	0.0% (0)	0.0% (0)	0.0% (0)	0.0% (0)	0.0% (0)	16.46% (26)	83.54% (132)
6A	Milwaukee	0.0% (0)	0.0% (0)	0.0% (0)	0.0% (0)	0.0% (0)	22.34% (44)	77.66% (153)
7	Fargo	0.0% (0)	0.0% (0)	0.0% (0)	0.0% (0)	0.0% (0)	5.91% (11)	94.09% (175)
8	Fairbanks	0.0% (0)	0.0% (0)	0.0% (0)	0.0% (0)	0.0% (0)	4.23% (3)	95.77% (68)
Arid								
2B	Phoenix	0.52% (1)	0.0% (0)	1.55% (3)	4.12% (8)	47.94% (93)	28.87% (56)	17.01% (33)
3B	Las Vegas	0.0% (0)	0.0% (0)	0.0% (0)	0.69% (1)	43.06% (62)	47.92% (69)	8.33% (12)
4B	Albuquerque	0.0% (0)	0.0% (0)	0.0% (0)	0.0% (0)	19.77% (34)	65.7% (113)	14.53% (25)
5B	Denver	0.0% (0)	0.0% (0)	0.0% (0)	0.0% (0)	8.14% (7)	50.0% (43)	41.86% (36)
6B	Helena	0.0% (0)	0.0% (0)	0.0% (0)	0.0% (0)	5.17% (6)	24.14% (28)	70.69% (82)
Marine								
3Bc	Los Angeles	0.94% (1)	0.0% (0)	0.0% (0)	0.94% (1)	28.3% (30)	16.04% (17)	53.77% (57)
3C	San Jose	0.0% (0)	0.0% (0)	0.0% (0)	0.62% (1)	4.35% (7)	13.66% (22)	81.37% (131)
4C	Seattle	0.0% (0)	0.0% (0)	0.0% (0)	0.0% (0)	0.0% (0)	10.97% (17)	89.03% (138)

References

(1) Angell, C. A. Relaxation in Liquids, Polymers and Plastic Crystals — Strong/Fragile Patterns and Problems. *Journal of Non-Crystalline Solids* **1991**, *131–133*, 13–31. https://doi.org/10.1016/0022-3093(91)90266-9.

(2) Shiraiwa, M.; Ammann, M.; Koop, T.; Pöschl, U. Gas Uptake and Chemical Aging of Semisolid Organic Aerosol Particles. *PNAS* **2011**, *108* (27), 11003–11008. https://doi.org/10.1073/pnas.1103045108.

(3) Price, H. C.; Mattsson, J.; Murray, B. J. Sucrose Diffusion in Aqueous Solution. *Phys. Chem. Chem. Phys.* **2016**, *18* (28), 19207–19216. https://doi.org/10.1039/C6CP03238A.

(4) Cummings, B. E.; Li, Y.; DeCarlo, P. F.; Shiraiwa, M.; Waring, M. Indoor Aerosol Water Content and Phase State in U.S. Residences: Impacts of Relative Humidity, Aerosol Mass and Composition, and Mechanical System Operation. *Environ. Sci.: Processes Impacts* **2020**. https://doi.org/10.1039/D0EM00122H.

(5) Evoy, E.; Maclean, A. M.; Rovelli, G.; Li, Y.; Tsimpidi, A. P.; Karydis, V. A.; Kamal, S.; Lelieveld, J.; Shiraiwa, M.; Reid, J. P.; Bertram, A. K. Predictions of Diffusion Rates of Large Organic Molecules in Secondary Organic Aerosols Using the Stokes–Einstein and Fractional Stokes–Einstein Relations. *Atmospheric Chemistry and Physics* **2019**, *19* (15), 10073–10085. https://doi.org/10.5194/acp-19-10073-2019.

(6) Pankow, J. F. An Absorption Model of Gas/Particle Partitioning of Organic Compounds in the Atmosphere. *Atmospheric Environment* **1994**, *28* (2), 185–188. https://doi.org/10.1016/1352-2310(94)90093-0.

(7) Cappa, C. D.; Jimenez, J. L. Quantitative Estimates of the Volatility of Ambient Organic Aerosol. *Atmospheric Chemistry and Physics* **2010**, *10* (12), 5409–5424. https://doi.org/10.5194/acp-10-5409-2010.

(8) Canagaratna, M. R.; Jimenez, J. L.; Kroll, J. H.; Chen, Q.; Kessler, S. H.; Massoli, P.; Hildebrandt Ruiz, L.; Fortner, E.; Williams, L. R.; Wilson, K. R.; Surratt, J. D.; Donahue, N. M.; Jayne, J. T.; Worsnop, D. R. Elemental Ratio Measurements of Organic Compounds Using Aerosol Mass Spectrometry: Characterization, Improved Calibration, and Implications. *Atmospheric Chemistry and Physics* **2015**, *15* (1), 253–272. https://doi.org/10.5194/acp-15-253-2015.

(9) Rackes, A.; Waring, M. S. Modeling Impacts of Dynamic Ventilation Strategies on Indoor Air Quality of Offices in Six US Cities. *Building and Environment* **2013**, *60*, 243–253. https://doi.org/10.1016/j.buildenv.2012.10.013.

(10) Touchie, M. F.; Siegel, J. A. Residential HVAC Runtime from Smart Thermostats: Characterization, Comparison, and Impacts. *Indoor Air* **2018**, *28* (6), 905–915. https://doi.org/10.1111/ina.12496.

(11) Waring, M. S. Secondary Organic Aerosol in Residences: Predicting Its Fraction of Fine Particle Mass and Determinants of Formation Strength. *Indoor Air* **2014**, *24* (4), 376–389. https://doi.org/10.1111/ina.12092.

(12) Weisel, C. P.; Zhang, J. (Jim); Turpin, B. J.; Morandi, M. T.; Colome, S.; Stock, T. H.; Spektor, D. M.; Korn, L.; Winer, A.; Alimokhtari, S.; Kwon, J.; Mohan, K.; Harrington, R.; Giovanetti, R.; Cui, W.; Afshar, M.; Maberti, S.; Shendell, D. Relationship of Indoor, Outdoor and Personal Air (RIOPA) Study: Study Design, Methods and Quality Assurance/Control Results. *J Expo Sci Environ Epidemiol* **2005**, *15* (2), 123–137. https://doi.org/10.1038/sj.jea.7500379.

(13) Stephens, B.; Siegel, J. A.; Novoselac, A. Operational Characteristics of Residential and Light-Commercial Air-Conditioning Systems in a Hot and Humid Climate Zone. *Building and Environment* **2011**, *46* (10), 1972–1983. https://doi.org/10.1016/j.buildenv.2011.04.005.

(14) Ben-David, T.; Rackes, A.; Waring, M. S. Alternative Ventilation Strategies in U.S. Offices: Saving Energy While Enhancing Work Performance, Reducing Absenteeism, and Considering Outdoor Pollutant Exposure Tradeoffs. *Building and Environment* **2017**, *116*, 140–157. https://doi.org/10.1016/j.buildenv.2017.02.004.

(15) Nguyen, J. L.; Schwartz, J.; Dockery, D. W. The Relationship between Indoor and Outdoor Temperature, Apparent Temperature, Relative Humidity, and Absolute Humidity. *Indoor Air* **2014**, *24* (1), 103–112. https://doi.org/10.1111/ina.12052.
(16) Nguyen, J. L.; Dockery, D. W. Daily Indoor-to-Outdoor Temperature and Humidity Relationships: A Sample across Seasons and Diverse Climatic Regions. *International Journal of Biometeorology; Heidelberg* **2016**, *60* (2), 221–229. http://dx.doi.org.ezproxy2.library.drexel.edu/10.1007/s00484-015-1019-5.